https://doi.org/10.1007/s11467-024-1426-3

RESEARCH ARTICLE

Generation and characterization of customized Laguerre–Gaussian beams with arbitrary profiles

Chengyuan Wang[1,*,†], Yun Chen[1,2,*], Jinwen Wang[1], Xin Yang[1], Hong Gao[1,‡], Fuli Li[1]

[1] Ministry of Education Key Laboratory for Nonequilibrium Synthesis and Modulation of Condensed Matter, Shaanxi Province Key Laboratory of Quantum Information and Quantum Optoelectronic Devices, School of Physics, Xi'an Jiaotong University, Xi'an 710049, China
[2] Department of Physics, Huzhou University, Huzhou 313000, China
*These authors contributed equally to this work.
Corresponding authors. E-mail: †wcy199202@gmail.com, ‡honggao@mail.xjtu.edu.cn
Received October 10, 2023; accepted February 1, 2024

Supporting Information

1. Experimental setup

The experimental setup is illustrated in Fig. S1. A horizontally polarized Gaussian beam (780 nm, Toptica DL) is perpendicularly incident on an SLM (HDSLM80R-PLUS) loaded with a pre-calculated hologram carrying the complex amplitude information of the target light field $\mathcal{A}\tilde{U}_0$. The beam diffracted from SLM is then spatially filtered by a filtering system composed of two lenses (with focal lengths of f1 = 250 mm and f2 = 150 mm respectively) and an iris, and its transverse intensity is recorded by a CCD (Lumenera INFINITY 3). The position of the CCD can also be shifted through a translation stage to record the intensity patterns at different propagation distances. The intensity patterns can be synthesized into a three-dimensional intensity volume, with an additional dimension representing the propagation distance. Each intensity volume is normalized by its maximum value, as shown in Fig. 3(a)-(f) in the manuscript. During the intensity recording process, it is always ensured that the CCD is not overexposed and the exposure time and gain are maintained, and each intensity pattern is averaged 5 times to minimize random errors. Besides, an additional reference beam can be switched on by a shutter (S) to interfere with the customized beams for phase measurements.

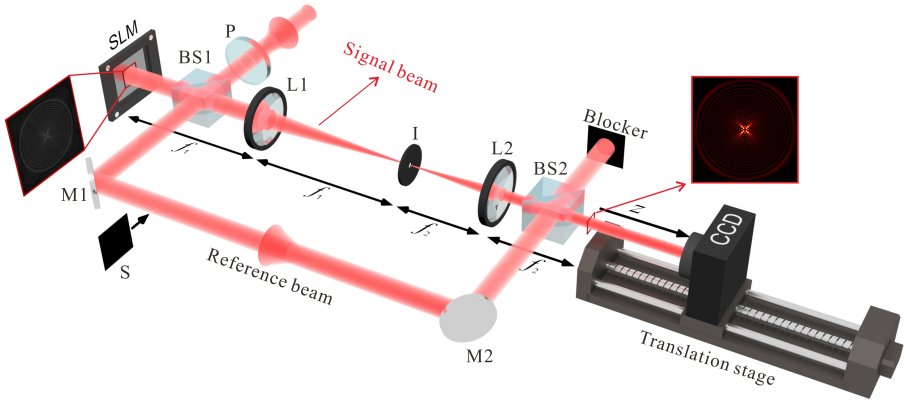

Fig. S1 Experimental setup. P: polarizer; L1-L2: lenses; M1-M2: mirrors; BS1-BS2: beam splitters; SLM: spatial light modulator; S: shutter; CCD: charge-coupled device.

2. Intensity and phase of experimentally customized light fields

We use a reference beam to interfere with the customized beams and record the interference patterns, then apply the holographic interferometry method [1] to determine the phase distributions of the customized beams, as shown in the second and fourth columns of Fig. S2. The intensity profiles of the object beams are also reconstructed for comparison, as shown in the first and third columns of Fig. S2. All the experimental and theoretical (see Fig. 1(b)) results are in good agreement, indicating that the qualities of the customized beams are very well.

Fig. 3(a)-(f) illustrates the 3-dimensional normalized intensity volume of the customized beams. Here we further give the transverse intensities of the corresponding beams at 5 different propagation distances, as shown in Fig. S3.

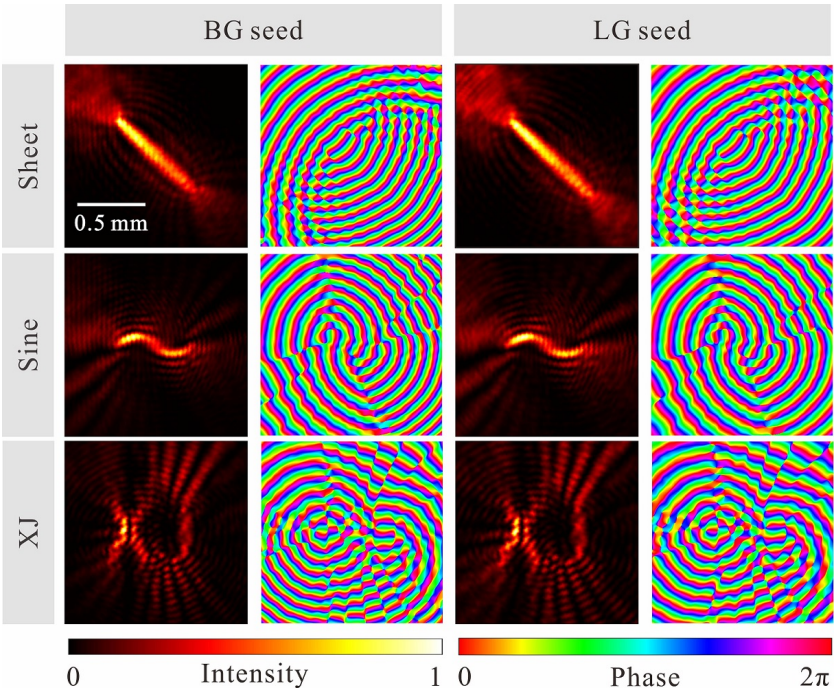

Fig. S2 Experimentally measured transverse intensities and phases of the customized beams.

3. Propagation of astroid-BG/LG and deltoid-BG/LG beams

Figure S4 shows the transverse intensity of astroid-BG/LG and deltoid-BG/LG beams propagating to 0, 0.5 z_{max}, z_{max}. Here, the spectrum modulation is set to $\mathcal{A} = \exp[i(5\sin(2\varphi)/2)]$ for the astroid-BG/LG beams and $\mathcal{A} = \exp[i5\sin(\varphi)^3]$ for the deltoid-BG/LG beams. It can be seen that similar to the results revealed in Fig. 3, the astroid-BG (or deltoid-BG) and astroid-LG (or deltoid-LG) initially have very similar intensity distributions due to undergoing the same spectrum modulation. But after transmission to the farthest distance, the latter still maintains clear shapes, although its outline is slightly expanded, while the former almost disappears in the field of view.

4. THeoretical simulations of the customized-BG/LG beams propagation in free space

The customized beam is obtained by acting a linear differential operator $\hat{\mathrm{A}}\left(D_x, D_y\right)$ on a seed beam $U_0(r,z)$. $\hat{\mathrm{A}}\left(D_x, D_y\right)$ can be expressed as a sum of products of derivatives [2]

$$\hat{\mathrm{A}}\left(D_x, D_y\right) \equiv C_{a,b} D_x^a D_y^b, \tag{S1}$$

where D_x^a and D_y^b are the ath-order and the bth-order derivatives with respect to x and y, $C_{a,b}$ is amplitude coefficient. $U_0(r,z)$ is a solution of the paraxial wave equation (PWE) and $\hat{\mathrm{A}}\left(D_x, D_y\right)$ commutates with the operator of the PWE. So $U(\mathbf{r},z) = \hat{\mathcal{A}}U_0(r,z)$ is a new solution of the PWE. Let $\mathcal{F}$ and $\mathcal{F}^{-1}$ represent the two-dimensional Fourier transform and inverse Fourier transform, and $U(\mathbf{r},z) = \hat{\mathcal{A}}U_0(r,z)$ can be rewritten in Fourier space as

$$U = \mathcal{F}^{-1}\left\{\mathcal{F}\left\{\hat{\mathcal{A}}U_0\right\}\right\} = \mathcal{F}^{-1}\left\{\mathcal{A}\mathcal{F}\left\{U_0\right\}\right\} = \mathcal{F}^{-1}\left\{\mathcal{A}\tilde{U}_0\right\}, \tag{S2}$$

where $\tilde{U}_0$ is the Fourier transforms U_0, and $\mathcal{A}$ is an algebraic function that represents the operator $\hat{\mathcal{A}}$ on the Fourier plane. A typical example related to $\hat{\mathcal{A}}$ is the ladder operator $\hat{\mathcal{L}}^{\pm} = \partial_x \pm i\partial_y$, with its algebraic function being $\mathcal{L}^{\pm} = \mathcal{F}[\hat{\mathcal{L}}^{\pm}] = -ik_x \pm k_y \propto k_r \exp(\pm i\phi)$, where $(k_x, k_y) = (k_r\cos\phi, k_r\sin\phi)$ represents Fourier coordinates. It can be verified that the operator $\hat{\mathcal{L}}^{\pm}$, when

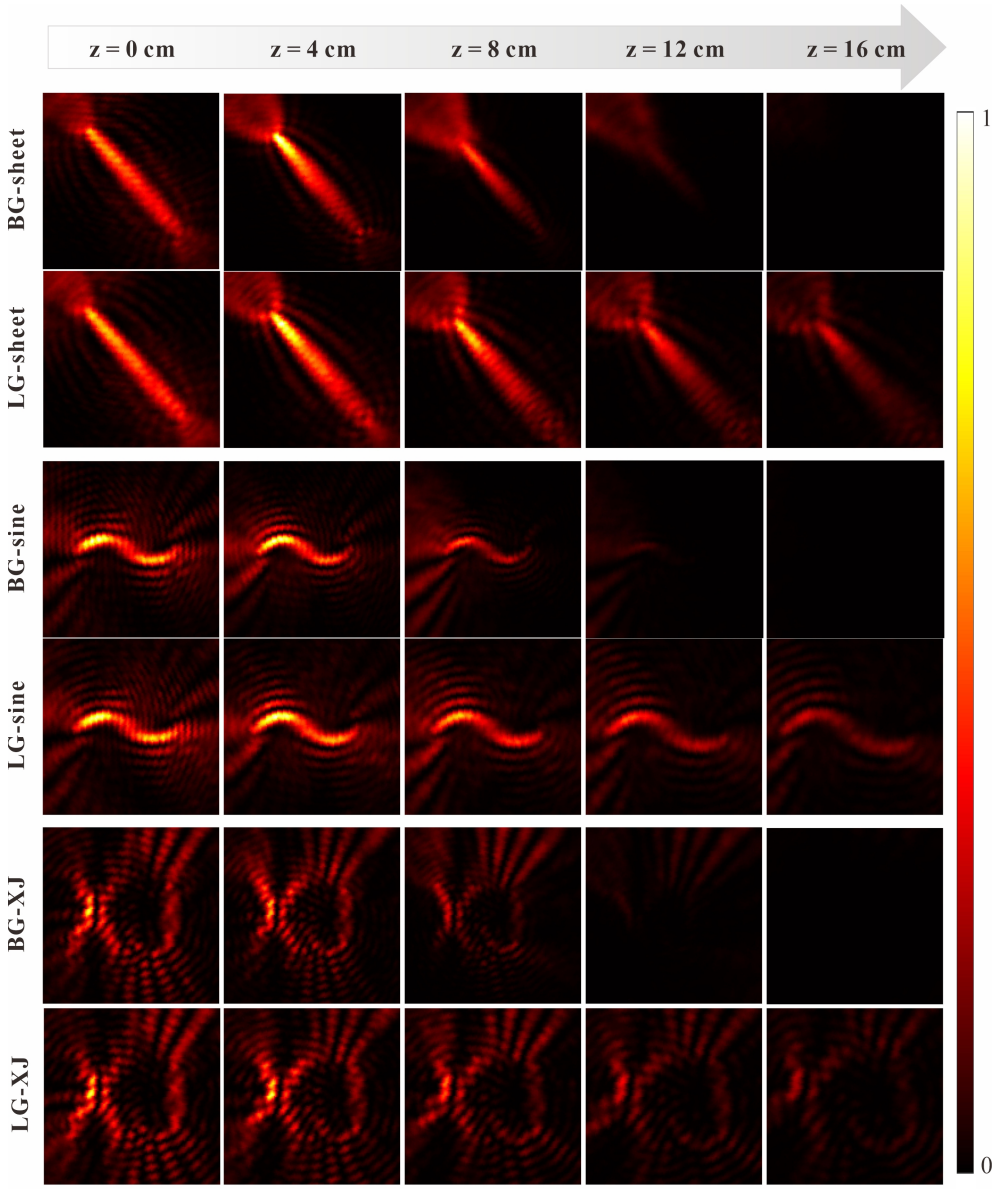

Fig. S3 Normalized intensity distribution in the $x-y$ plane of customized light fields at various propagation distance z.

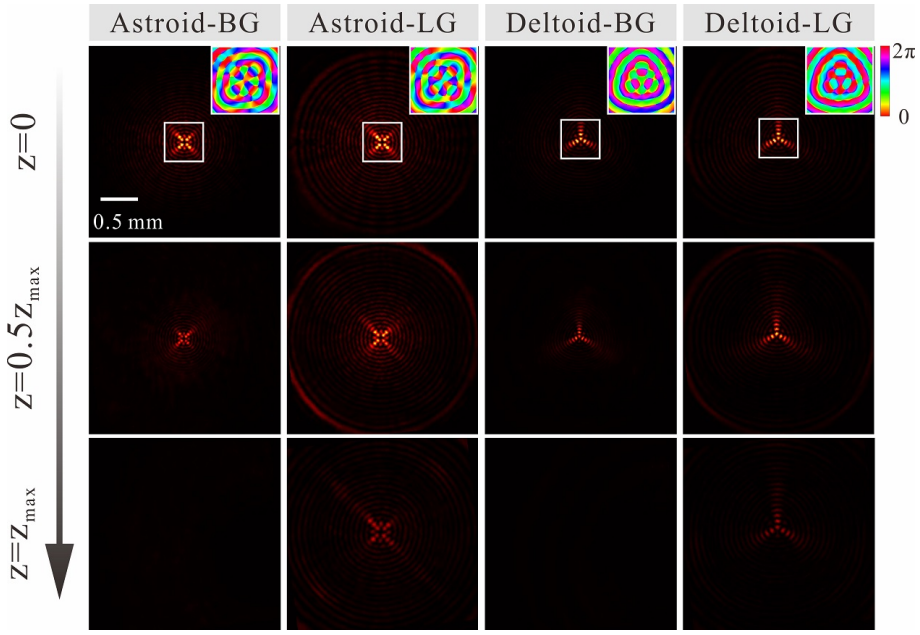

Fig. S4 Transverse intensity of the customized beams at different propagation distances. The inset reveals the phase corresponding to the region indicated by the white box.

applied to the 0th-order Bessel beam with wavenumber k_t, yields the 1st-order Bessel beam, i.e., $\hat{\mathcal{L}}^{\pm} J_0(k_t r) = \mathcal{F}^{-1}[\mathcal{L}^{\pm}\mathcal{F}[J_0(k_t r)]] \propto \mathcal{F}^{-1}[\delta(k_r - k_t)\exp(\pm i\phi)] \sim J_1(k_t r)\exp(\pm i\phi)$.

An arbitrary field $U(\mathbf{r})$ with diffraction-free properties can be expressed using Whittaker's integration

$$U(\mathbf{r}) = \oint \mathcal{A}(\varphi)\exp[ik_t \mathbf{r}\cdot\mathbf{u}(\varphi)]d\varphi, \tag{S3}$$

where $\mathcal{A}(\varphi)$ is the algebraic function employed to modulate the shape of $U(\mathbf{r})$, k_t represents the transverse wavenumber, $\mathbf{u}(\varphi) = (\cos\varphi, \sin\varphi)$ is a unit vector related to the azimuthal angle. When $\mathcal{A} = 1$, $U(\mathbf{r})$ corresponds to the 0th-order Bessel beam (denoted as U_{B0}) and locates at the origin of coordinates. If we aim to shift the center of U_{B0} to the position $\mathbf{r} = \mathbf{r}_c$, $\mathbf{r}$ in Eq. (6) should be replaced by $(\mathbf{r} - \mathbf{r}_c)$. The optical field after this movement is represented by

$$U_{B0}(\mathbf{r} - \mathbf{r}_c) = \oint \exp[ik_t(\mathbf{r} - \mathbf{r}_c)\cdot\mathbf{u}(\varphi)]d\varphi. \tag{S4}$$

Comparing Eq. (6) and Eq. (7), we can observe that the algebraic function $\mathcal{A}$, corresponding to the 0th-order Bessel beam with the field center located at $\mathbf{r} = \mathbf{r}_c$, is $\mathcal{A} = \exp[-ik_t\mathbf{r}_c\cdot\mathbf{u}(\varphi)]$. When we use U_{B0} as a 'pencil' and continuously shift it along a preset curve $\mathbf{r}_c(\tau)$, then the corresponding $\mathcal{A}$ should be integrated over the curve, i.e., $\int_{\mathbf{r}_c(\tau)}\exp[-ik_t\mathbf{r}_c\cdot\mathbf{u}(\varphi)]d\tau$. However, it should be mentioned that the superposition of the 0th-order Bessel beam along the aforementioned curve may impact the shape of the customized beam, which is undesirable. Hence, it is necessary to introduce an additional phase term γ_B into the integral. By utilizing the generalized law of refraction [3], it can be established that for a customized beam using a pre-defined curve $\mathbf{r}_c(\tau)$, its intensity profile r_c satisfies $r_c = \frac{1}{k_t}\frac{d\arg[\mathcal{A}(\varphi)]}{d\varphi}$, where $\arg[x]$ is the angle phase of x. Consequently, it can be inferred from a simple example, such as when $\mathbf{r}_c$ represents a circular ring, resulting in $\arg[A] = 2\pi r_c k_t = k_t \oint |\mathbf{r}_c(s)|ds$, that γ_B should be proportional to the arc length of the curve $\mathbf{r}_c$: $\gamma_B(\tau) = k_t\int_0^\tau |\mathbf{r}_c(s)|ds$. Incorporating all the above analyses, we can obtain the mathematical description of $\mathcal{A}$ corresponding to the target curve $\mathbf{r}_c(\tau)$

$$\mathcal{A}(\varphi) = \int_{\mathbf{r}_c}\exp[i\gamma_B(\tau) - ik_t\mathbf{r}_c\cdot\mathbf{u}(\varphi)]d\tau. \tag{S5}$$

We use the theory above, as well as the scalar diffraction theory and fast Fourier transform algorithm [4] to simulate the propagation of the customized beams shown in Fig. 3. The calculated

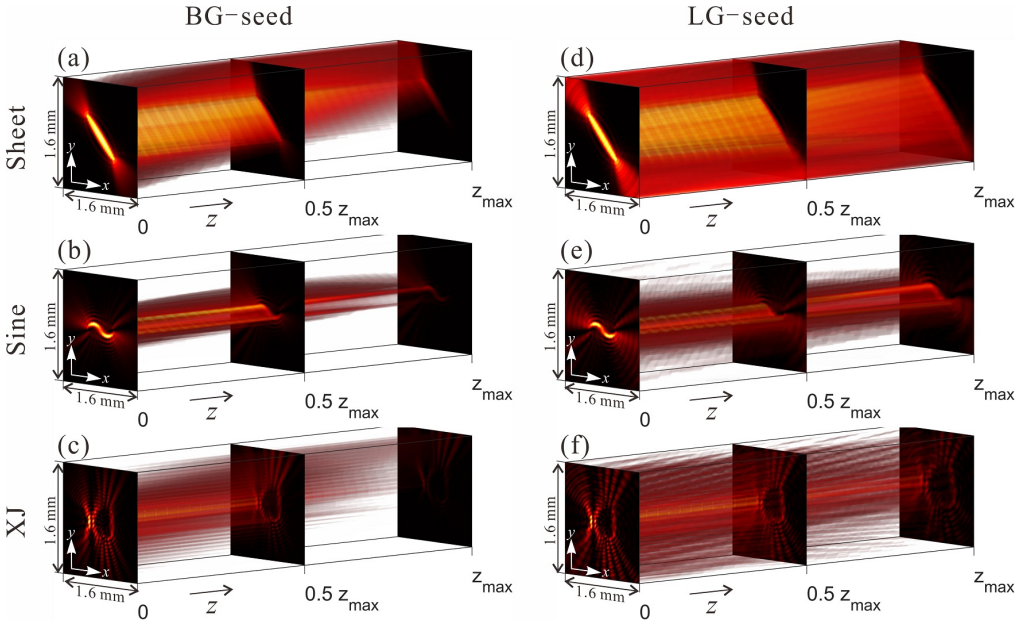

Fig. S5 Theoretical normalized intensity volume for (a)-(c) customized-BG and (d)-(f) customized-LG beams.

normalized intensity volume is displayed in Fig. S5, from which we can see that compared with the customized-LG beams, the customized-BG with similar spatial structure experienced more serious intensity attenuation during propagation, which is consistent with the experimental results given in Fig. 3.

We also give a qualitative analysis of why the intensity of the customized-LG beams decays slower than that of the customized-BG beams, as detailed below. The customized optical field can be regarded as an ordered superposition of the seed beams. Therefore, the intensity attenuation rate of the customized beam is similar to that of the seed beams. Given that the intensity of the seed beam is highly localized to the center point, the intensity decay phenomenon can be comprehended by analyzing the on-axis intensity variation with the propagation distance of the seed beam. From the general expression of LG beams, the on-axis field of an LG seed (when $l = 0$) satisfies

$$LGU_0(r = 0, z) \propto \frac{1}{\omega_0 \sqrt{1 + (z/z_r)^2}} L_p^0(0), \tag{S6}$$

where $z_r = \pi\lambda\omega_0^2$ is the Rayleigh length, equivalent to z_{max} as mentioned in our main text. From Eq. (S6), we can further derive the on-axis intensity of the LG seed as

$$I_{LG}(r = 0, z) \propto \frac{1}{1 + (z/z_r)^2}. \tag{S7}$$

Regarding the BG seed beams described by Eq. (4) in the manuscript, its amplitude of the electric field evolving with propagation distance z is typically given by [5]

$$|BU_0(r, z)| = A \frac{\omega_B}{\omega(z)} J_0 \left[k_t r/(1 + iz/z_{Br})\right] \exp\left[-r^2/\omega^2(z) + k_t^2 z^2/k^2\right], \tag{S8}$$

where $z_{Br} = \pi\lambda\omega_B^2$ and $\omega(z) = \omega_B\sqrt{1 + (z/z_{Br})^2}$. Hence, we obtain the on-axis intensity of the BG seed as

$$I_{BG}(r = 0, z) = |BU_0(r = 0, z)|^2 \propto \frac{1}{1 + (z/z_{Br})^2} \left[\exp\left(-\frac{k_t^2 z^2}{k^2\omega^2(z)}\right)\right]^2. \tag{S9}$$

Considering that z is within the range of 0 to z_r (or z_{max}) and $\omega_B = \sqrt{2N}\omega_0 \gg \omega_0$ (since $N = p + 1/2 \gg 1$), it follows that $z/z_{Br} \leq z_r/z_{Br} = (\omega_0/\omega_B)^2 \ll 1$, thereby resulting in

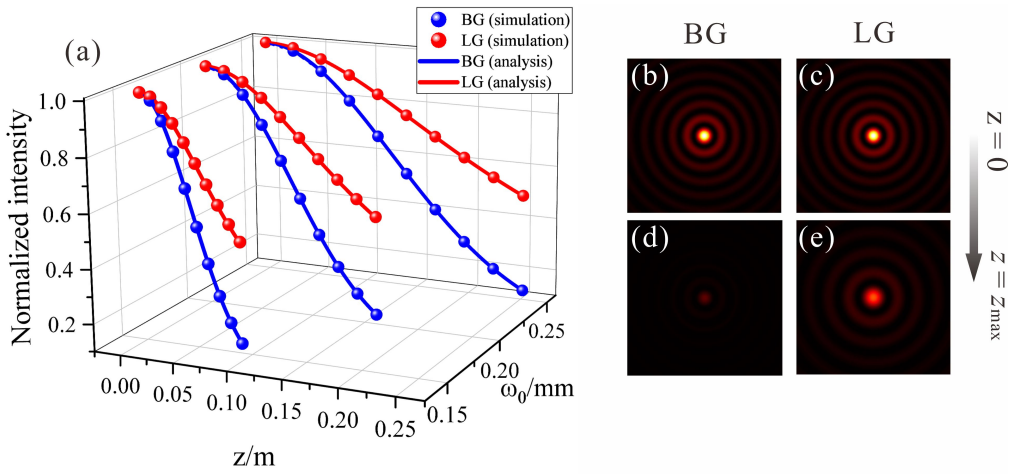

Fig. S6 (a) The on-axis intensity variation with propagation distance z for two seed beams under different waist sizes ω_0. (b-e) Normalized intensity of BG and LG beams with $\omega_0 = 0.25$ mm at $z = 0$ [(b) and (c)] and $z = z_{max}$ [(d) and (e)]. The simulations are performed with the parameter set to $p = 20$ and $\lambda = 780$ nm.

$1 + (z/z_{Br})^2 \approx 1$ and $\omega(z) \approx \omega_B$. Incorporating these approximations with the relationship of $k_t = 2\sqrt{2N}/\omega_0$ and $\omega_B = \sqrt{2N}\omega_0$, Eq. (S9) can be simplified to the form:

$$I_{BG}(r = 0, z) \propto \exp(-z^2/z_r^2). \tag{S10}$$

Comparing Eq. (S7) and Eq. (S10), we can see that $I_{LG}(r = 0, z) \geq I_{BG}(r = 0, z)$ consistently holds for $0 \leq z \leq z_r$. This means that the intensity attenuation rate of the LG seed is slower than that of the BG seed, regardless of the values of ω_0 and p. Using the analytical formula (i.e., Eq. (S6) and (S9)) and the angular spectrum propagation method, we obtain the variations of $I_{BG}(r = 0, z)$ and $I_{LG}(r = 0, z)$ with the propagation distance under different ω_0, as shown in Fig. (S6). This trend is consistent with that of the customized beam in the manuscript.

References

1. G. T. Nehmetallah, R. Aylo, and L. Williams, *Analog and Digital Holography with MATLAB* (SPIE, 2015).
2. I. Martinez-Castellanos and J. C. Gutiérrez-Vega, "Shaping optical beams with non-integer orbital-angular momentum: a generalized differential operator approach," Opt. Lett. **40**, 1764–1767 (2015).
3. N. Yu, P. Genevet, M. A. Kats, F. Aieta, J.-P. Tetienne, F. Capasso, and Z. Gaburro, "Light propagation with phase discontinuities: Generalized laws of reflection and refraction," Science **334**, 333–337 (2011).
4. D. G. Voelz, *Computational fourier optics: a MATLAB tutorial* (SPIE, 2011).
5. F. Gori, G. Guattari, and C. Padovani, "Bessel-gauss beams," Opt. Commun. **64**, 491–495 (1987).